processes

MDPI

Article

Transient Energy-Based Ultra-High-Speed Unit Protection for Overhead Outgoing Lines in Inverter-Interfaced Renewable Energy Plants

Yuan Kong *, Yumeng Wu, Zhenfeng Liang and Rong Jia

Department of Electrical Engineering, Xi'an University of Technology, Xi'an 710048, China
* Correspondence: yolandaxaut@foxmail.com

Abstract: The transient fault characteristics of an inverter-interfaced renewable energy (IIRE) overhead outgoing line may cause misoperations of existing protection schemes. This paper uses directional comparison of the post-fault transient energy to construct the ultra-high-speed (UHS) unit protection for an IIRE plant's overhead outgoing line. The proposed method could identify the internal faults accurately in various fault scenarios. Compared to conventional traveling wave-based protection, distance protection and differential protection, the proposed scheme can overcome the high sampling rate difficulty and remain effective when the fault inception angle is zero. The scheme is also tested under conditions of noise, parallel lines, and CT saturation. The simulation results demonstrate that the proposed method is immune to these factors, which make the scheme more reliable and applicable in commercial industries.

Keywords: inverter-interfaced renewable energy (IIRE); overhead outgoing line protection; post-fault energy; directional protection

Academic Editor: Mohan Lal Kolhe

Received: 12 November 2024
Revised: 12 December 2024
Accepted: 13 December 2024
Published: 20 January 2025

Citation: Kong, Y.; Wu, Y.; Liang, Z.; Jia, R. Transient Energy-Based Ultra-High-Speed Unit Protection for Overhead Outgoing Lines in Inverter-Interfaced Renewable Energy Plants. *Processes* **2025**, *13*, 286. https://doi.org/10.3390/pr13010286

1. Introduction

To address the increasingly severe energy crisis and environmental challenges, IIRE technologies, such as wind and photovoltaic power generation, have made great progress in recent years. By 2024, the cumulative installed capacity for wind power and photovoltaic systems is projected to reach 467 million kW and 714 million kW, respectively. This growth will lead to a rising proportion of IIRE —particularly represented by permanent magnet direct-drive wind turbines and photovoltaic systems. However, the increasing deployment of power electronic equipment has introduced changes in the system's fault characteristics [1,2]. The weak feed conditions, time-varying impedance and disparities between positive and negative sequence impedances have brought about many challenges to the conventional protection of an IIRE plant's overhead outgoing line. As a result, these traditional protection schemes may fail to operate correctly [3,4].

Numerous studies were conducted on the adaptive analysis of distance protection of overhead outgoing line in an IIRE plant. Despite these improvements in conventional distance protection, they still could not reach an acceptable reliability in correctly identifying internal faults [5–9]. Unlike traditional synchronous generators, IIRE has short-circuit currents with limited amplitude and controlled phase angles, which can cause distance protection to misoperate. Distance protection is based on power frequency components, so it needs at least one full cycle (20 ms) to respond, leading to slower operation.

Differential protection, as one of the conventional protection schemes of IIRE's outgoing line, is largely affected by renewable energy fault characteristics, leading to risks of

maloperation. Renewable energy sources create weak fault signals, which reduce the sensitivity of conventional differential protection. According to references [10–12], conventional current differential protection may misoperate due to phase distortion and limited fault amplitude when renewable energy is connected to a weakly synchronized system.

Traveling wave protection is another approach for transmission line protection, which is based on fault propagation characteristics [13–16]. References [17–21] identify fault direction by analyzing the polarities of voltage and current traveling waves. Additionally, the fault direction can be evaluated based on the amplitudes or energies of forward and reverse traveling waves [22–24]. Furthermore, references [25–28] introduce the concept of composite surge impedance, defined as the ratio of the first voltage traveling wave to the first current traveling wave, which is used to determine the fault direction. However, challenges arise from the difficulty of capturing the wave head and the need for a high sampling rate [29], which make these protection schemes not reliable when the fault inception angle is zero [30,31]. In summary, traveling wave-based protection relies on the detection of the initial traveling wave head and requires a very high sampling rate, making it difficult to be implemented in the industry.

This paper proposes a UHS unit protection of the overhead outgoing line of an IIRE plant based on transient energy. The principle of this method is easy to implement and the sampling rate is 10 kHz, which makes it more reliable and more applicable in commercial industries.

2. Materials and Methods

2.1. Analysis of Post-Fault Transients in IIRE Plant's Overhead Outgoing Line

The schematic diagram of a typical IIRE plant's overhead outgoing line is shown in Figure 1, where G_1~G_n, respectively, represent the equivalent sources of the IIRE wind turbine in the wind farm; the length of the collection line in wind farm is generally no more than 20 km. In general, the voltage level of the collection bus is 35 kV. In China, the voltage level of the overhead outgoing line is 220 kV or 330 kV, and the voltage level of the transmission line RT is 500 kV or 750 kV. f_1 and f_2 are fault locations and Line SP is the protected line.

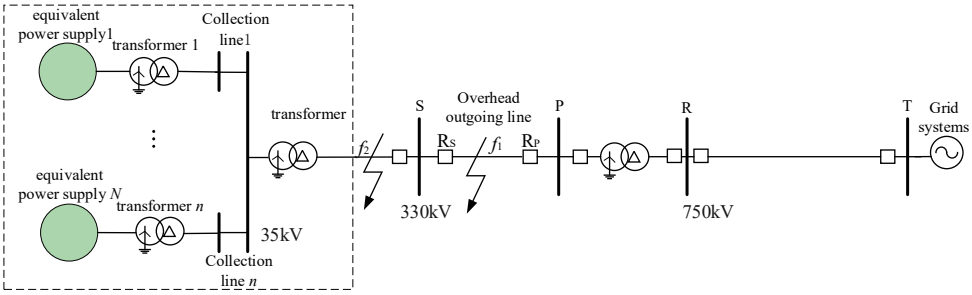

Figure 1. Schematic diagram of typical IIRE plant's overhead outgoing line fault.

The weak feeding characteristics of the IIRE makes the fault current of the overhead outgoing line smaller compared to the fault current of the grid system. Here, an A-G fault occurs at the midpoint of Line SP, the phase A current waveforms of Terminal S and P is shown in Figure 2, and Figure 3 is obtained after spectral analysis, from which it can be seen that most of the energy is concentrated in the 50 Hz bandwidth, but a large amount of energy still exists in the high frequency bandwidth, which contains rich post-fault information [21,32]. These transients are carried by the traveling waves of currents and voltages, whose propagation is shown in Figure 4 [33].

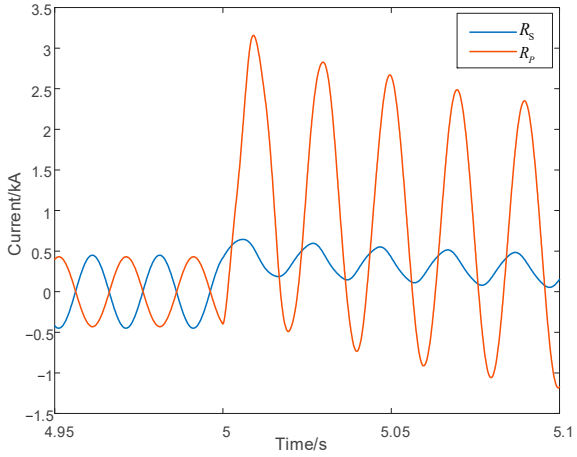

Figure 2. The phase A current of Terminal S and P in the event of faults.

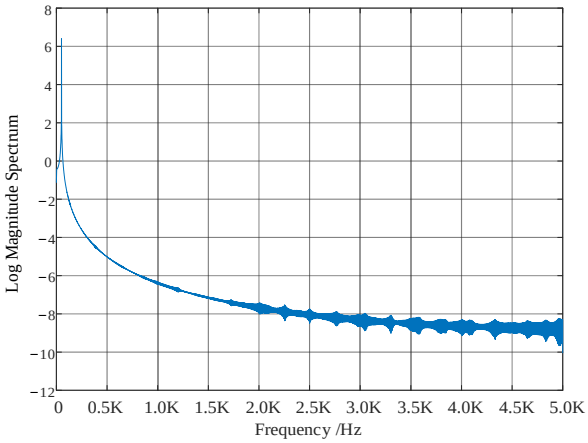

Figure 3. Spectral analysis of fault currents on wind farm side of map.

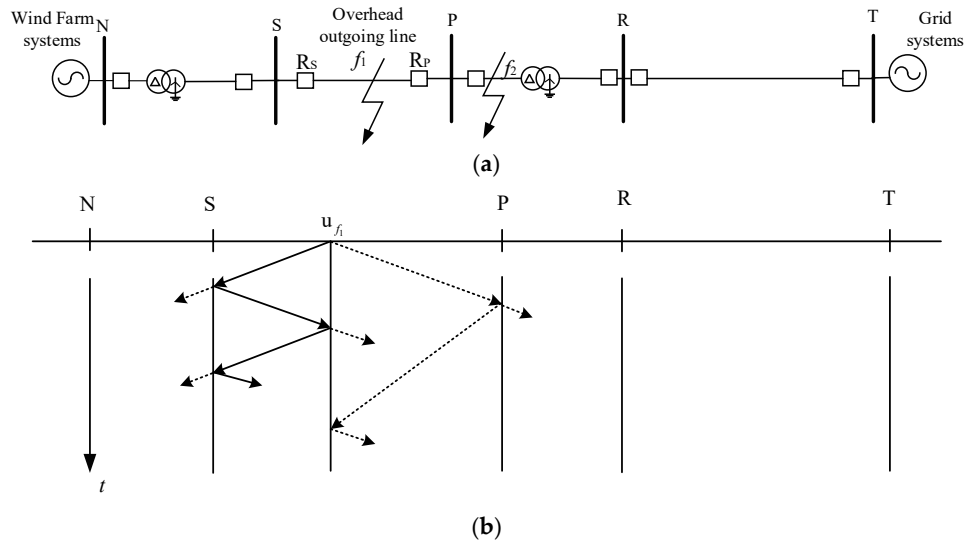

Figure 4. Schematic diagram: (**a**) typical IIRE plant's overhead outgoing line fault, (**b**) propagation of traveling waves.

2.2. UHS Unit Protection Algorithm of IIRE Plant's Overhead Outgoing Line

As discussed in Section II-A, the post-fault transients can be utilized to construct a novel protection scheme. This paper utilizes the post-fault transient energy to form the protection scheme, and the detailed principle is illustrated as follows.

The system of Figure 1 is simplified to a steady-state overhead outgoing system as shown in Figure 4a, and according to the superposition theorem, the post-fault superposition network is shown in Figures 5 and 6, where Figure 5 indicates a forward fault and Figure 6 indicates a reverse fault. The following analysis is based on an A-G fault in a single-phase system, and the principle can be applied to a three-phase system by means of the Karenbauer transform [21].

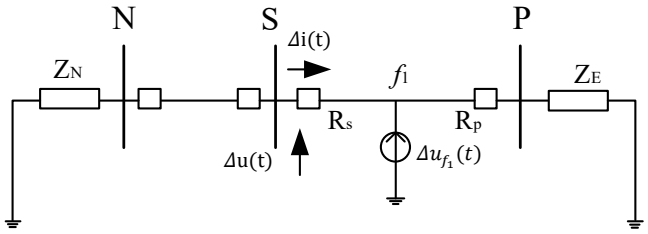

Figure 5. The superposition network under a forward fault.

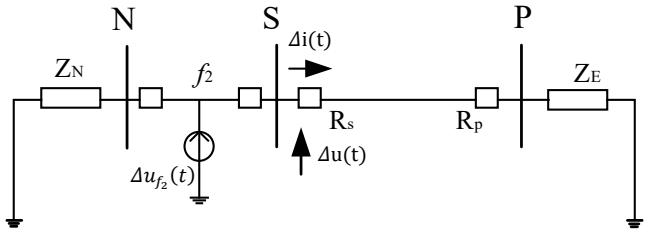

Figure 6. The superposition network under a reverse fault.

The current flowing outward from the bus is specified as its positive direction. For relay R_s, the positive direction is the flow from bus S to the P side. The transient energy is calculated as follows:

$$P(t) = \Delta u(t)\Delta i(t) \tag{1}$$

$$S_{R_S} = \int_{t_1}^{t_1+\tau} P(t)\mathrm{d}t \tag{2}$$

where $\Delta u(t)$ and $\Delta i(t)$ indicate the calculated superimposed voltage and current, $P(t)$ is the transient power, t_1 is the time at which the initial traveling wave arrives at the relay, and τ represents the data window. As shown in Figure 5 for a positively oriented fault, S_1 and S_{L_1}, respectively, denote the energy absorbed by Z_N and Line NS after the fault, and Z_N is the equivalent impedance of the wind farm system to the bus N. Thus,

$$S_{R_S} = -S_1 - S_{L_1} \tag{3}$$

For reverse direction faults, we obtain

$$S_{R_P} = S_2 + S_{L_2} \tag{4}$$

where S_2 and S_{L_2} represent the energy absorbed by Z_E and the Line SP after a fault, respectively. Z_E is the equivalent impedance of the gride system to the bus P. S_1, and S_2, S_{L_1}, and S_{L_2} are all positive.

Take the following system as an example, for relay R_s, if $R_s < 0$, set $S_{R_{flag}} = 1$, otherwise $S_{R_{flag}} = 0$; this logic applies to the other relay R_P as well.

The protection scheme presented in this paper is illustrated in Figure 7. Firstly, the relays at the two terminals of the protected line collect the voltage and current measurement samples.

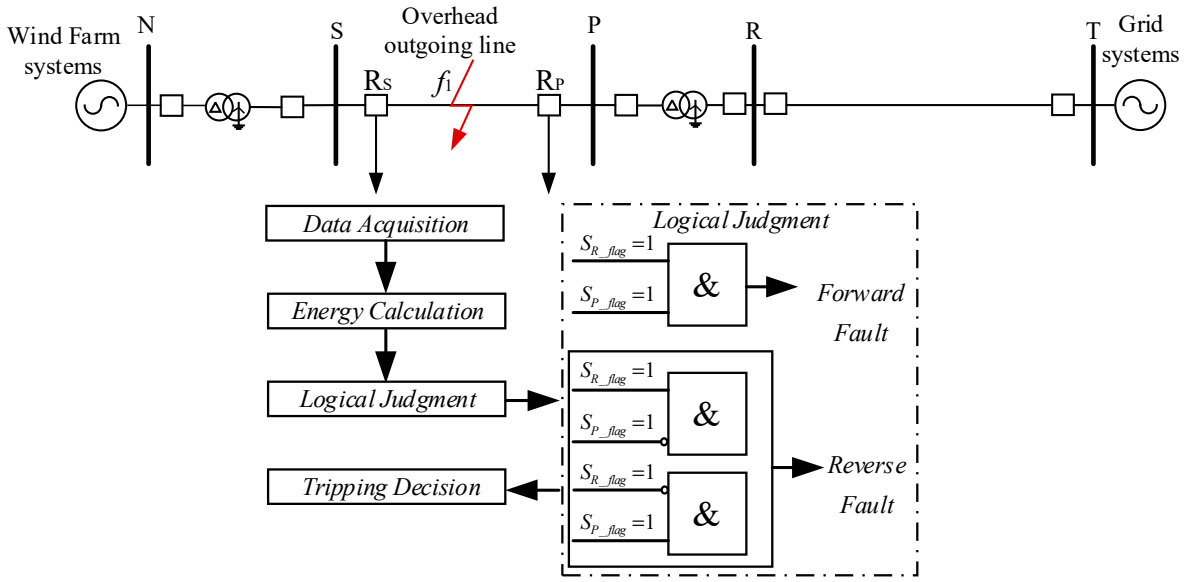

Figure 7. Block diagram of overall protection scheme.

Secondly, the three-phase currents and voltages are decoupled by Karenbauer's phase-to-mode transformation, which is shown in Equation (5).

Thirdly, the post-fault transient energy of both terminals is calculated via Equation (2).

Finally, the direction is compared to identify whether the fault is internal or external, according to the logical judgment shown in Figure 7.

$$\boldsymbol{T}_{0,\alpha,\beta}^{a,b,c} = \begin{bmatrix} 1 & 1 & 1 \\ 1 & -2 & 1 \\ 1 & 1 & -2 \end{bmatrix} \tag{5}$$

If a positive direction fault is detected in both sides of the protected line, it indicates that the fault is internal. Otherwise, the fault is identified as an external one.

3. Results

In this section, the performance of the proposed method is discussed, and tests are conducted under different scenarios.

3.1. Simulation Model

In PSCAD/EMTDC, the IIRE plant's system shown in Figure 1 is constructed, including 100 equivalent IIRE sources. The configuration of the overhead outgoing line is shown in Figure 8, and a frequency-dependent model is used. The rated capacity of the IIRE plant is 200 MW, and the system frequency is 50 Hz. The wind farm side is connected to the grid system through the transformer, which is boosted to 330 kV, and then further boosted to 750 kV, and the stray capacitance on the busbar is 0.01 μF. The sampling rate of the relay R_s in Figure 1 is 10 kHz. The overhead outgoing Line SP is the protected line and f_1, f_2 denote the fault location on different line segments, respectively.

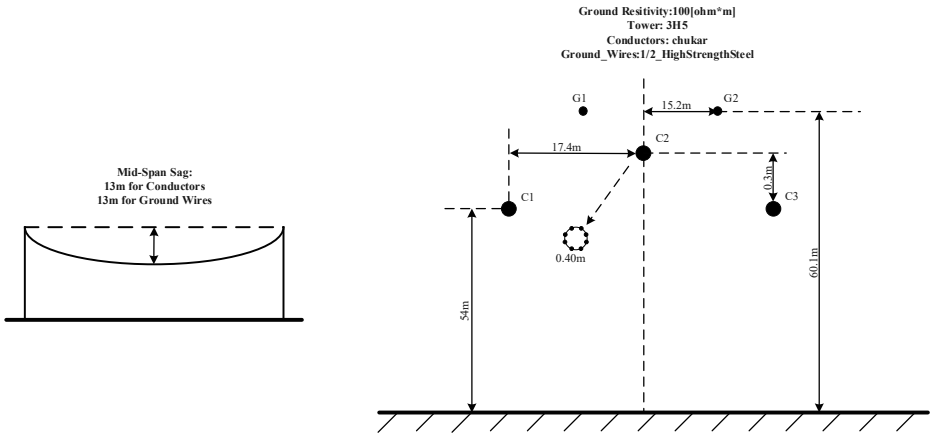

Figure 8. Line configuration of overhead outgoing line.

3.2. Simulation Verification

(1) Simulation of Typical Faults: It is assumed that an A-G fault occurs at f_1, at a distance of 20 km from the bus S, with a fault inception angle of 45°, with a fault resistance of 100 Ω. $S_{R_S} = -499.48$ kJ < 0 and $S_{R_P} = -7355.6$ kJ < 0. Since the transient energy absorbed on both sides is negative, the fault is identified as a forward fault; therefore, it is determined to be the internal fault. Here, an A-G fault occurs at a distance of 50 km from the bus R, with a fault inception angle of 45° and with a fault resistance of 100 Ω, $S_{R_S} = -6074.1$ kJ < 0 and $S_{R_P} = 601.92$ kJ >0. It can be seen that the fault is a forward fault for bus S, a reverse fault for bus P. In this case, the fault is identified as an external one. To verify the impact of fault types on the proposed method, extensive simulations were conducted in this study, and the results showing in Figure 9 indicate that the method is immune to the fault type.

(2) Effect of Fault Location: To verify the effect of fault location on the proposed method, set the fault type as an A-G fault, with the fault inception angle of 0°, and a fault resistance of 100 Ω. From Figure 10, it can be seen that the protection operates correctly regardless of whether it is an internal fault or a close-in fault. In addition, the fault location in Figure 10a means that the fault occurs in the line length from bus R, and in Figure 10b, the fault occurs in the line length from bus S.

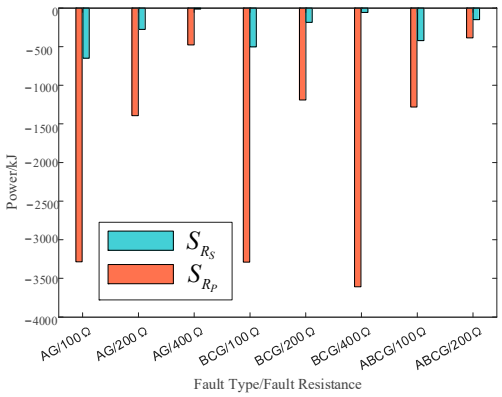

(**a**)

Figure 9. *Cont.*

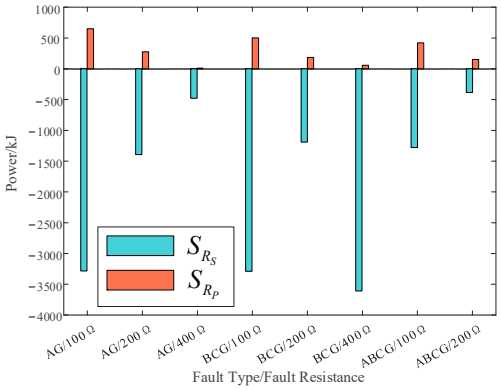

(**b**)

Figure 9. Fault identification results of different fault types: (**a**) Internal Fault, (**b**) External Fault.

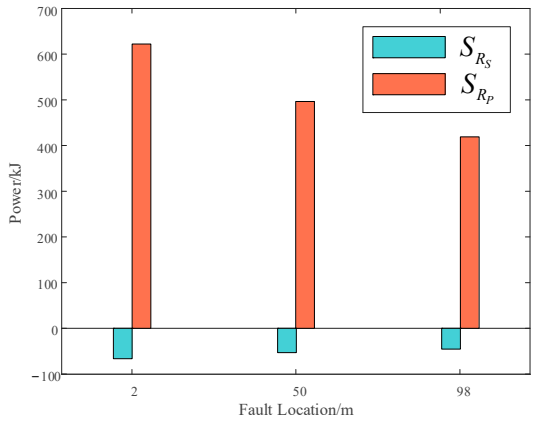

(**a**)

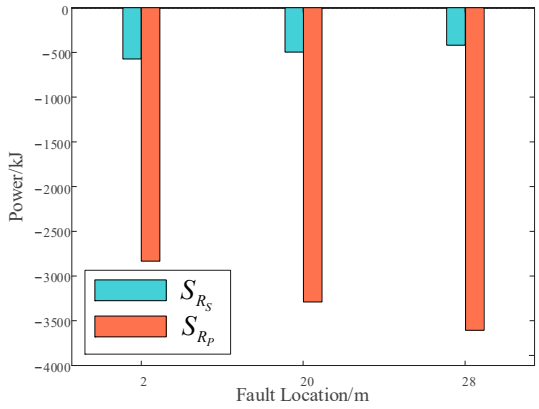

(**b**)

Figure 10. Fault identification results of different fault locations: (**a**) External Fault, (**b**) Internal Fault.

(3) Effect of Fault Inception Angle: According to references [22–27], it can be seen that conventional traveling wave-based protection is largely affected by the fault inception angle. However, the proposed method is not affected by the fault inception angle and remains effective even when the fault inception angle is zero. When setting the fault resistance as 100 Ω, Figure 11 shows the results for various fault inception angles and different fault types. Obviously, the final result is immune to the fault inception angle.

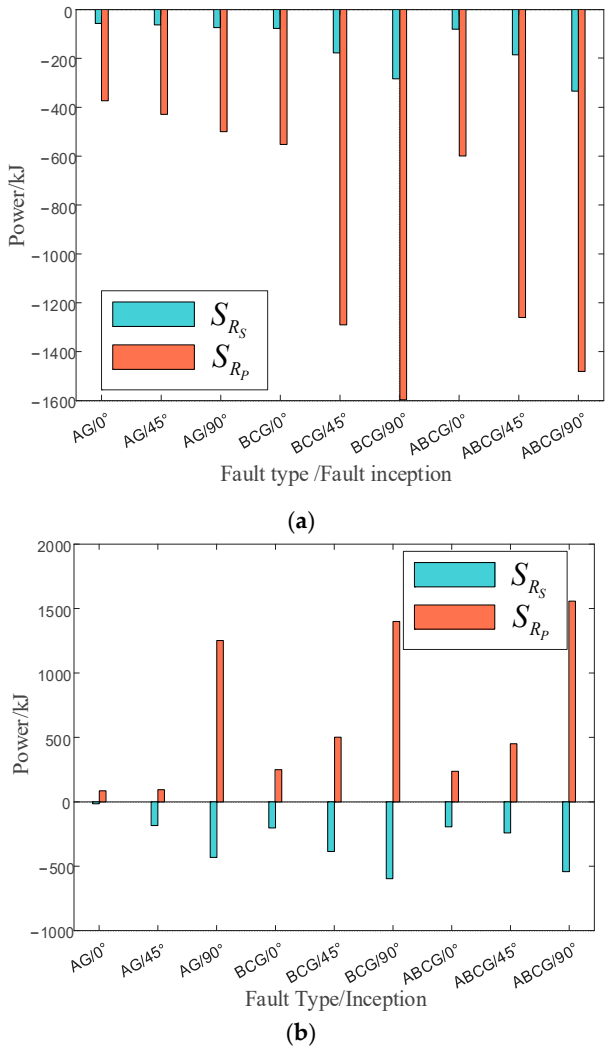

Figure 11. Fault identification results of different fault inception angle: (**a**) Internal Fault, (**b**) External Fault.

(4) Effect of Fault Resistance: The simulation results are carried out in the case where the fault resistance is 100/200/400 Ω, respectively. It is obvious from Figure 12 that the proposed method can identify the internal fault, and it is immune to fault resistance.

(5) Effect of Parallel Line System: This section discusses the performance of the proposed method in a parallel line system. The system is set up in PSCAD, as shown in Figure 13. Fault f1 and f2, respectively, represent an internal fault and external fault and are all at the midpoint of the line. An A-G fault occurs with a fault inception angle of 45°, and a fault resistance of 50 Ω. Here, the fault occurs at f1, and the transient energies calculated on both sides of the Line SP are $S_{R_S} = -259.3752$ kJ and $S_{R_P} = -398.2975$ kJ. Here, the fault occurs at f2, and the transient energies are $S_{R_S} = 103.5088$ kJ and $S_{R_P} = -99.7948$ kJ. Thus, it can effectively identify the internal fault.

(6) Effect of Current Transformer (CT) Saturation: CT saturation typically occurs at the half cycle after fault inception and will lead to distortion in current samples. The conventional fundamental frequency-based methods usually suffer from CT saturation and may misoperate in such scenarios. However, the proposed method is based on the propagation characteristics of traveling waves, which travel at the speed of light. The length of an IIRE plant's overhead outgoing line generally does not exceed a few tens of kilometers. Even if the fault occurs at the farthest end, the sample time window of the

proposed method will not exceed 2 ms. At this point, saturation has not yet occurred, which means the proposed method is naturally not affected by CT saturation.

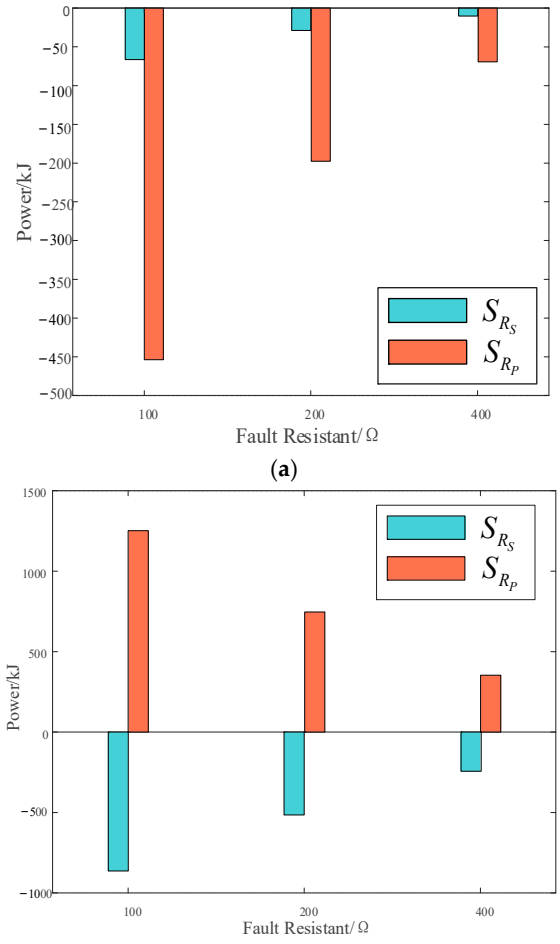

Figure 12. Fault identification results of different fault resistances: (**a**) Internal Fault, (**b**) External Fault.

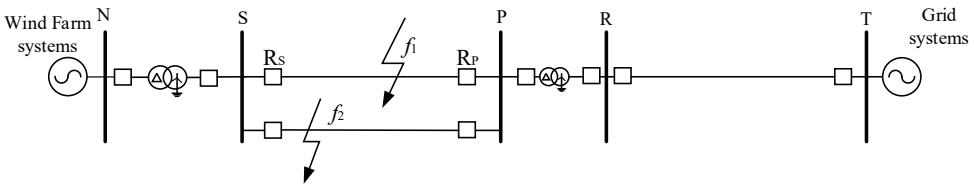

Figure 13. IIRE plant's overhead outgoing line with parallel line system model.

Here, an internal and external A-G fault are used as examples to show this advantage. The fault occurs at a distance of 20 km from bus S. As shown in Figure 14a, the current transformer is saturated, and the secondary samples have obvious distortion. The transient energy on each side of the line is $S_{R_S} = -189.7596$ kJ and $S_{R_P} = -48.5937$ kJ, indicating an internal fault.

An external A-G fault occurs at f2, with a distance of 20 km from bus P. Similarly, as shown in Figure 14b, the current transformer is saturated, and the secondary samples are obviously distorted. The transient energy calculated on both sides of the line is $S_{R_S} = -36.7459$ kJ and $S_{R_P} = 43.6396$ kJ. Thus, the fault is determined as external.

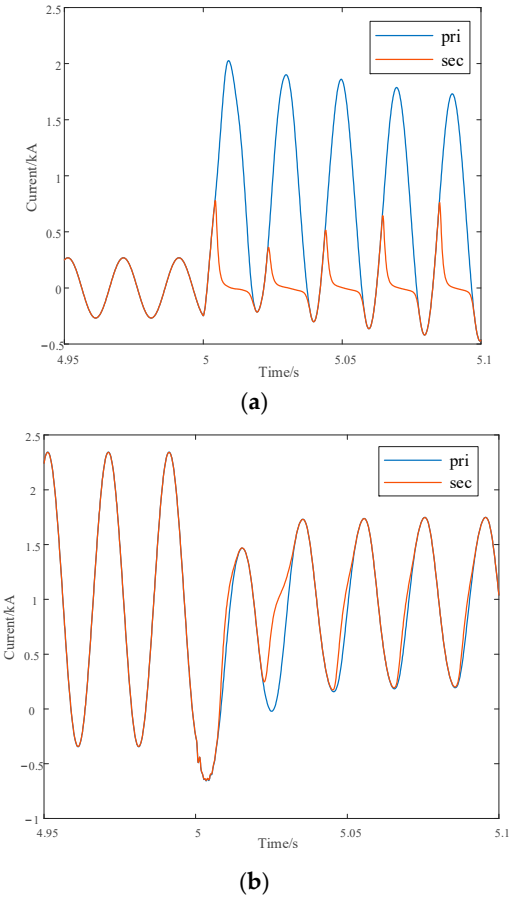

Figure 14. CT primary and secondary side currents on overhead outgoing line under (**a**) an internal A-G fault and (**b**) an external A-G fault.

(7) Effect of Noise: The impact of noise on the proposed method is discussed in this section. An A-G fault is set at f1 on the overhead outgoing line, with a distance of 20 km from bus S. The white noise of 20 dB is added to the measurement samples. The transient energies calculated on both sides of the Line SP are $S_{R_S} = -98.1793$ kJ and $S_{R_P} = -495.25973$ kJ, which indicates the fault is internal. If the fault occurs at f2, with a distance of 20 km from bus R, the transient energies calculated on both sides of the Line SP are $S_{R_S} = -125.7254$ kJ and $S_{R_P} = 139.8637$ kJ. The fault is correctly determined as external. Therefore, the proposed method has a good tolerance of noise.

3.3. Comparison of Proposed Method with Traditional Protection

(1) Distance protection: The basic principle of distance protection is to identify the fault by determining the impedance from the sending terminal of the line to the fault point. The measured impedance $\dot{Z}_{\mathrm{m}}$ is calculated as in Equation (6) and the threshold impedance $\dot{Z}_{set}$ is set as in Equation (7) [34].

$$\dot{Z}_{\mathrm{m}} = \frac{\dot{U}_S}{\dot{I}_S} \tag{6}$$

$$\dot{Z}_{set} = K_{rel}\dot{Z}_{sp} \tag{7}$$

where $\dot{Z}_{sp}$ is the impedance of Line SP, and the reliability coefficient K_{rel} is typically set as 0.85 [9]. The protection logic is as follows: if $\left|\dot{Z}_{\mathrm{m}}\right| > \left|\dot{Z}_{set}\right|$, the fault is treated as external; otherwise, if $\left|\dot{Z}_{\mathrm{m}}\right| \leq \left|\dot{Z}_{set}\right|$, the fault is treated as internal.

Here, an internal A-G fault occurs on the overhead outgoing line at a distance of 20 km from bus S. According to the distance protection scheme described above, $\left|\dot{Z}_{set}\right| = 4557.7$, $\left|\dot{Z}_{\mathrm{m}}\right| = 5389.5$. Since $\left|\dot{Z}_{\mathrm{m}}\right| > \left|\dot{Z}_{set}\right|$, the distance relay will incorrectly treat this fault as external.

In contrast, the transient energy is calculated on both sides of Line SP, $S_{R_S} = -334.2178$ kJ < 0 and $S_{R_P} = -1232.1436$ kJ < 0; therefore, the proposed method is able to correctly identify the fault as internal.

(2) Differential protection: Its action equation is shown as follows [35]:

$$\begin{cases} I_{\mathrm{op}} > I_{\mathrm{op},0} I_{\mathrm{res}} \leqslant I_{\mathrm{res},0} \\ I_{\mathrm{op}} \geqslant I_{\mathrm{op},0} + kI_{\mathrm{res}} I_{\mathrm{res}} > I_{\mathrm{res},0} \end{cases} \tag{8}$$

where $I_{\mathrm{op}} = \left|I_1 + I_2\right|$, $I_{\mathrm{res}} = \left|I_1 - I_2\right|$, I_1, I_2 are the currents on both sides of the protected line. Take the following Figure 15 as an example: if the calculated result falls into the action area, the fault is identified as internal, otherwise the fault is identified as external.

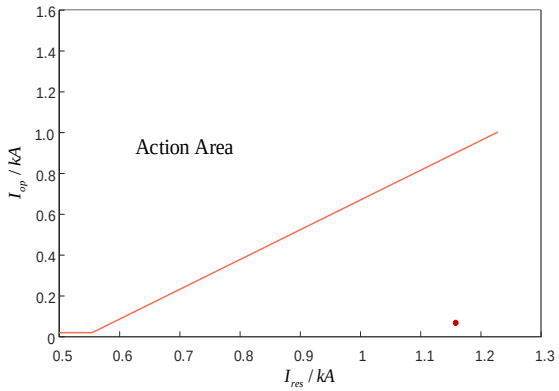

Figure 15. Operational result of differential protection.

In the IIRE system, the limitation of the short circuit current further leads to the differential current amplitude close to the braking current amplitude. The weak feeding characteristics of IIRE in the power system make this phenomenon even more pronounced. In cases of higher fault resistance and smaller fault inception angles, the short circuit current is even smaller. Since the differential protection only utilizes power frequency component information for protection, which contains limited fault information, it usually misoperates in the IIRE system.

The proposed method utilizes transient information over a broad frequency bandwidth, and thus it could achieve higher sensitivity and enable faster fault identification.

Here, an internal A-G fault occurs on the overhead outgoing line, at a distance of 20 km from bus S, and differential current protection is used to identify the fault. The action result is shown in Figure 15. However, the result shows that the fault is incorrectly identified as external. In contrast, the transient energy calculated on each side of Line SP is $S_{R_S} = -177.4918$ kJ < 0 and $S_{R_P} = -1250.3568$ kJ < 0; therefore, the proposed method can correctly identify the fault as internal.

4. Conclusions

This paper uses the directional comparison of post-fault transient energy to construct the UHS unit protection for an IIRE plant's overhead outgoing line. The fault is determined by discussing the polarity of the transient energy on both sides of the line. Compared to conventional traveling wave-based protection, the proposed method is able to overcome the high sampling rate difficulty and remain effective when the fault inception angle is zero. Various scenarios were tested in this study, including fault type, fault resistance, and

fault location. The results show that the proposed method is immune to these factors. The scheme is further tested in the presence of noise, parallel lines, and CT saturation, and the simulation results show that the proposed method is still effective. These advantages make the proposed method more reliable and applicable in commercial industries.

Author Contributions: Conceptualization, Y.K.; Methodology, Y.K. and Y.W.; Software, Y.K. and Y.W.; Validation, Y.K. and Y.W.; Formal Analysis, Y.K. and Y.W.; Investigation, Y.K. and Y.W.; Data Curation, Y.K. and Y.W.; Writing—Original Draft Preparation, Y.K. and Y.W.; Writing—Review and Editing, Y.K. and Y.W.; Visualization, Y.K. and Y.W.; Supervision, Y.K., Z.L. and R.J.; Project Administration, Y.K., Z.L. and R.J.; Funding Acquisition, Y.K., Z.L. and R.J. All authors have read and agreed to the published version of the manuscript.

Funding: This research received no external funding.

Data Availability Statement: Data are contained within the article.

Conflicts of Interest: The authors declare no conflicts of interest. The funders had no role in the design of the study; in the collection, analyses, or interpretation of the data; in the writing of the manuscript; or in the decision to publish the results.

References

1. Wilches-Bernal, F.; Bidram, A.; Reno, M.J.; Hernandez-Alvidrez, J.; Barba, P.; Reimer, B.; Montoya, R.; Carr, C.; Lavrova, O. A Survey of Traveling Wave Protection Schemes in Electric Power Systems. *IEEE Access* **2021**, *9*, 72949–72969. [CrossRef]
2. Jia, K.; Yang, Z.; Fang, Y.; Bi, T.; Sumner, M. Influence of inverter-interfaced renewable energy generators on directional relay and an improved scheme. *IEEE Trans. Power Electron.* **2019**, *34*, 11843–11855. [CrossRef]
3. Yang, Z.; Jia, K.; Li, Z.; Zhao, H.; Fang, Y.; Feng, T.; Liu, B. Adaptability Analysis of the Directional Relay for the System with Inverter-interfaced Renewable Energy Generators. In Proceedings of the 2019 IEEE 8th International Conference on Advanced Power System Automation and Protection (APAP), Xi'an, China, 21–24 October 2019; pp. 1611–1616.
4. Song, G.; Chang, P.; Hou, J.; Zhang, C.; Lyu, J. Adaptability Analysis of Fault Component Directional Component in AC/DC Multi-terminal Infeed System. *Autom. Electr. Power Syst.* **2021**, *45*, 136–145.
5. Jia, K.; Yang, Z.; Bi, T.; Li, Y. Impact of Inverter-Interfaced Renewable Energy Generators on Distance Protection and an Improved Scheme. In Proceedings of the 2019 IEEE Power & Energy Society General Meeting (PESGM), Atlanta, GA, USA, 4–8 August 2019; p. 1.
6. Jieyu, C.; Zhen, T.; Jun, L. Influence of impedance characteristics of wind power supply on phasor-based distance protection. *Smart Power* **2018**, *46*, 63–68.
7. Li, B.; Zhou, B.H.; He, J.W.; Li, B.; Li, Y. Applicability analysis of distance protection with positive-sequence voltage polarization for transmission lines of wind farm with directdriven turbines. *Autom. Electr. Power Syst.* **2023**, *47*, 16–24.
8. Wang, C.; Song, G.; Tang, H.; Chi, Y.; Chang, Z.; Li, D. Adaptability analysis of distance protection in power system integration with wind farms. *Autom. Electr. Power Syst.* **2015**, *39*, 10–15.
9. Fang, Y.; Jia, K.; Yang, Z.; Li, Y.; Bi, T. Impact of inverter interfaced renewable energy generators on distance protection. *Power Syst. Prot. Control* **2018**, *46*, 54–59.
10. Li, Y.; Jia, K.; Bi, T.; Sun, Y.; Li, W. Adaptability analysis of current differential protection of outgoing transmission line emanating from invert-interfaced renewable energy power plants. *Autom. Electr. Power Syst.* **2017**, *41*, 100–105.
11. Yang, G.; Dong, M.; Zhou, Z.; Zhou, C.; Du, D.; Zhan, Z.; Yang, D. The influences and countermeasures of wind farm access to transmission line differential protection. In Proceedings of the 2012 IEEE Power Electronics and Machines in Wind Applications, Denver, USA, CO, USA, 16–18 July 2012; pp. 1–4.
12. Lai, Y.; Wang, Z.; Wang, T. Adaptability analysis of current differential protection in an AC power grid with an MMC-HVDC and improvement measures. *Power Syst. Prot. Control* **2023**, *51*, 145–154.
13. Kong, Y.; Zhang, B.; Hao, Z. Study of Ultra-High-Speed Protection of Transmission Lines Using a Directional Comparison Scheme of Transient Energy. *IEEE Trans. Power Deliv.* **2015**, *30*, 1317–1322. [CrossRef]
14. Duan, J.D.; Zhang, B.H.; Li, P.; Luo, S.B.; Xue, J.; Shi, M.H.; Cheng, L.Y. Principle and algorithm of non-unit transient-based protection for EHV transmission lines. *Proc. CSEE* **2007**, *27*, 45–51.
15. Zou, G.; Gao, H.; Zhu, F.; Wang, H. Realization scheme of directional unit protection based on travelling wave integral. In Proceedings of the 2011 4th International Conference on Electric Utility Deregulation and Restructuring and Power Technologies (DRPT), Weihai, China, 6–9 July 2011; pp. 73–77.

16. Chamia, M.; Liberman, S. Ultra high speed relayfor EHV/UHV transmission lines-development design and application. *IEEE Trans. Power App. Syst.* **1978**, *PAS-97*, 2104–2116. [CrossRef]
17. Dong, X.; Luo, S.; Shi, S.; Wang, B.; Wang, S.; Ren, L.; Xu, F. Implementation and application of practical traveling-wave-based directional protection in UHV transmission lines. *IEEE Trans. Power Del.* **2016**, *31*, 294–302. [CrossRef]
18. Chen, W.; Malik, O.P.; Yin, X.; Chen, D.; Zhang, Z. Study of wavelet-based ultra-high-speed directional transmission line protection. *IEEE Trans. Power Del.* **2003**, *18*, 1134–1139. [CrossRef]
19. Aguilera, C.; Orduna, E.; Ratta, G. Directional traveling-wave protection based on slope change analysis. *IEEE Trans. Power Del.* **2007**, *22*, 2025–2033. [CrossRef]
20. Dong, X.; Wang, S.; Shi, S. Polarized Current Travelling-wave Based Directional Relay. *Autom. Electr. Power Syst.* **2011**, *35*, 78–83.
21. Akimoto, Y.; Yamamoto, T.; Hosakawa, H.; Sakaguchi, T.; Yoshida, T.; Nishida, S. Fault protection based on travelling wave theory (Part I-theory). *Electr. Eng.* **1978**, *98*, 79–86. [CrossRef]
22. Bo, Z.Q.; Jiang, F.; Chen, Z.; Dong, X.Z.; Weller, G.; Redfern, M.A. Transient based protection for power transmission systems. In Proceedings of the 2000 IEEE Power Engineering Society Winter Meeting. Conference Proceedings (Cat. No.00CH37077), Singapore, 23–27 January 2000; Volume 3, pp. 1832–1837.
23. Crossley, P.A.; McLaren, P.G. Distance protection based on travelling waves. *IEEE Trans. Power App. Syst.* **1983**, *PAS-102*, 2971–2983. [CrossRef]
24. Johns, A.T.; Martin, M.A.; Barker, A.; Walker, E.P.; Crossley, P.A. A new approach to E.H.V. direction comparison protection using digital signal processing techniques. *IEEE Power Eng. Rev.* **1986**, *PER-6*, 28. [CrossRef]
25. Dong, X.; Kong, W.; Cui, T. Fault Classification and Faulted-Phase Selection Based on the Initial Current Traveling Wave. *IEEE Trans. Power Deliv.* **2009**, *24*, 552–559. [CrossRef]
26. Dong, X.; Ge, Y.; He, J. Surge impedance relay. *IEEE Trans. Power Del.* **2005**, *20*, 1247–1256. [CrossRef]
27. He, Z.; Liu, X.; Li, X.; Mai, R. A novel traveling-wave directional relay based on apparent surge impedance. *IEEE Trans. Power Del.* **2015**, *30*, 1153–1161. [CrossRef]
28. Prakash, K.S.; Malik, O.P.; Hope, G.S. High Speed Digital Directional Comparison Relaying. *Electr. Mach. Power Syst.* **1988**, *15*, 353–369. [CrossRef]
29. Aguilar, R.; Perez, F.; Orduna, E.; Rehtanz, C. The directional feature of current transients application in high-speed transmission-line protection. *IEEE Trans. Power Del.* **2013**, *28*, 1175–1182. [CrossRef]
30. Lei, A.; Dong, X.; Terzija, V. An Ultra-High-Speed Directional Relay Based on Correlation of Incremental Quantities. *IEEE Trans. Power Deliv.* **2018**, *33*, 2726–2735. [CrossRef]
31. Nayak, K.; Kumar, A. Pradhan Directional Relaying Applying Phase Quantities of Current Traveling Wave and Pre-fault Voltage. In Proceedings of the 2022 22nd National Power Systems Conference (NPSC), New Delhi, India, 17–19 December 2022; pp. 631–636.
32. Shi, Z.; Yu, J.; Ding, X. Research on transient protection based on time-frequency domain features. In Proceedings of the 2022 IEEE 5th International Conference on Automation, Electronics and Electrical Engineering (AUTEEE), Shenyang, China, 18–20 November 2022; pp. 186–190.
33. Yaozhong, G. *New Types Protective Relaying and Fault Location Theory and Techniques*; Xi'an Jiaotong University Press: Xi'an, China, 2007.
34. Zhang, B.; Li, G.; Wang, J.; Hao, Z.; Liu, Z.; Bo, Z. Affecting factors of grid connected wind power on fault current and impact on protection relay. *Electr. Power Autom. Equip.* **2012**, *32*, 1–8.
35. Zhang, B.; Wang, J.; Hao, Z. Impact of wind farm integration on relay protection (4): Performance analysis for wind farm outgoing transformer protection. *Electr. Power Autom. Equip.* **2013**, *33*, 1–8.